



Cite this: *Nanoscale*, 2014, 6, 13630

Flexible, thorn-like ZnO-multiwalled carbon nanotube hybrid paper for efficient ultraviolet sensing and photocatalyst applications

Dali Shao,^a Hongtao Sun,^b Jian Gao,^c Guoqing Xin,^b Mark Anthony Aguilar,^d Tiankai Yao,^b Nikhil Koratkar,^{b,c} Jie Lian^{*b} and Shayla Sawyer^{*a}

We report fabrication of a flexible, thorn-like ZnO-multiwalled carbon nanotube (MWCNT) hybrid paper with high aspect ratio for efficient ultraviolet (UV) sensing and photocatalyst applications. The thorn-like ZnO-MWCNT hybrid paper was synthesized *via* atomic layer deposition (ALD) of a uniform ZnO thin film on the outside surface of the MWCNT followed by hydrothermal growth of ZnO branches. The hybrid paper achieved very high surface to volume ratio, which is favorable for photodetector and photocatalyst applications. A photodetector fabricated from the hybrid paper demonstrates a high sensitivity to UV light with a maximum photoresponsivity of 45.1 A W⁻¹ at 375 nm, corresponding to an external quantum efficiency as high as 14927%. The rise time and fall time of the UV photodetector are 29 ms and 33 ms, respectively, indicating fast transient response characteristics for the device. The high photoresponsivity and fast transient response are attributed to efficient carrier transport and collection efficiency of the hybrid paper. Besides, the thorn-like ZnO-MWCNT hybrid paper demonstrates excellent photocatalytic performance under UV irradiation, enabling photo-degradation of organic dyes such as Rhodamine B (RhB) within 90 minutes, with good recyclability.

Received 12th July 2014,
Accepted 17th September 2014
DOI: 10.1039/c4nr03921a

www.rsc.org/nanoscale

1. Introduction

As a wide bandgap semiconductor material, ZnO has drawn significant research interest due to its unique optical and electrical properties including wide band gap (3.37 eV), large exciton binding energy (60 meV) at room temperature, low cost, and environmental friendliness.^{1,2} By virtue of these material properties, ZnO has been considered one of the most promising candidates for UV sensing and degradation of various organic pollutants.^{3–6} However, the performance of ZnO based UV photodetectors and photocatalysts is usually limited. For example, UV photodetectors fabricated from ZnO nanomaterials suffer poor transient response (on the order of minutes), and the efficiency of ZnO based photocatalysts is still not high enough for industrial applications.^{4,5} These performance limits mainly originate from the low carrier separation and transport efficiency in ZnO. Therefore, it is highly

desirable to develop a strategy to overcome these limits for fast UV sensing and efficient photocatalyst applications.

Composite nanomaterials have attracted tremendous research interests in recent years due to their multifunctional material properties. Carbon nanotube (CNT) has many remarkable material properties including high carrier transport mobility, superior mechanical properties and excellent chemical stability.^{7,8} The incorporation of CNT into the composites can provide them with the unique functions of CNT and also possibly induce intriguing properties that are inherited from synergistic effects.^{9,10} In particular, it has been reported that ZnO-CNT nanocomposites exhibit excellent performance in applications such as photocatalysts,¹¹ electron emitters,¹² field effect transistors,¹³ optical switches,¹⁴ and photodetectors.¹⁵ Thus far, various processes have been developed to fabricate ZnO-CNT nanocomposites, including electrochemical deposition,¹⁶ pulsed laser deposition,¹⁷ thermal chemical vapor deposition (CVD),¹⁸ covalent coupling,¹⁹ and water-assisted growth.²⁰ However, the growth of ZnO branches on CNT paper with ultrahigh aspect ratio remains a challenge, which is due to the difficulty in covering a thin and uniform ZnO seed layer over the complex surface of the CNT paper. One possible method to solve this issue is to take advantage of ALD which uses sequential self terminating gas–solid reactions for seed layer coating on extremely complex shapes with a conformal material layer of high quality.^{21–23}

^aDepartment of Electrical, Computer and Systems Engineering, Rensselaer Polytechnic Institute, Troy, NY 12180, USA. E-mail: sawyes@rpi.edu

^bDepartment of Mechanical, Aerospace and Nuclear Engineering, Rensselaer Polytechnic Institute, Troy, NY 12180, USA. E-mail: lianj@rpi.edu

^cDepartment of Materials Science and Engineering, Rensselaer Polytechnic Institute, Troy, NY 12180, USA

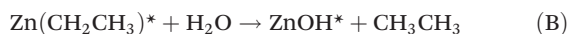
^dDepartment of Physics and Astronomy, California State University, Los Angeles, CA 90032, USA

In this work, we fabricated a flexible, thorn-like ZnO-multi-walled carbon nanotube (MWCNT) hybrid paper with high aspect ratio for efficient UV sensing and photocatalyst applications. The thorn-like ZnO-MWCNT hybrid paper was synthesized *via* ALD of a uniform ZnO seed layer on the exterior surfaces of the MWCNT followed by hydrothermal growth of ZnO branches. The hybrid paper achieved very high surface to volume ratio, which is favorable for photodetector and photocatalyst applications. A photodetector fabricated from the hybrid paper demonstrates a high photoresponsivity and a fast transient response in the UV region, which can be attributed to efficient carrier transport and collection efficiency of the hybrid paper. Besides, the thorn-like ZnO-MWCNT hybrid paper also demonstrates outstanding photocatalytic performance under UV irradiation, enabling photo-degradation of organic dyes such as RhB within a short time. The hybrid paper showed good recyclability as a photocatalyst, and could be used multiple times without performance degradation. Most importantly, the fabrication method in this work may open up new opportunities for fabrication of many other flexible, recyclable, and high performance functional devices for a wide range of applications including optical switching, hydrogen generation, gas sensing and energy storage.

2. Experimental

2.1 ALD of ZnO shell onto MWCNT paper

Commercial surface-functionalized MWCNT papers were obtained from Buckeye Composites Inc. A thin and uniform ZnO seed layer was deposited on MWCNT papers using a SUNALETM R-200 ALD-reactor. The ZnO ALD was performed using alternating diethylzinc and H₂O exposures:



where the asterisks represent the surface species. By repeating these reactions in an ABAB... sequence, ZnO layer can be deposited with atomic layer control. The ZnO ALD reaction sequence was: (i) dose diethylzinc to 1.0 Torr for 120 seconds; (ii) evacuate reaction products and excess diethylzinc; (iii) dose N₂ to 20.0 Torr for 60 seconds and then evacuate N₂ (repeat 5 times); (iv) dose H₂O to 1.0 Torr for 120 seconds, (v) evacuate reaction products and excess H₂O; (vi) dose N₂ to 20.0 Torr for 60 seconds and then evacuate N₂ (repeat 5 times). This sequence constitutes one AB cycle of ZnO ALD. The ZnO ALD was performed at 150 °C with 50 cycles.

2.2 Hydrothermal thermal synthesis of ZnO branches

Ammonium hydroxide (28 wt%) was added dropwise into 0.1 M zinc chloride solution until the pH is 10–11 and the solution was clear. Subsequently, the transparent solution was transferred to a Teflon-lined autoclave (Parr, USA) and the MWCNT paper coated with ZnO shell was suspended in the solution at 95 °C for 3 hours in a regular laboratory oven. Then

the growth solution was cooled down to room temperature naturally. The resulting substrate was thoroughly washed with deionized water and absolute ethanol for several times and dried in air at room temperature followed by post-annealing treatment in Ar/H₂ (ratio, 96:4) atmosphere at 400 °C for 2 hours.

2.3 Material characterization

A Carl Zeiss Ultra 1540 dual beam scanning electron microscope (SEM) was used to determine the morphology of the ZnO-MWCNT hybrid paper. Transmission electron microscopy (TEM) and high resolution TEM (HRTEM) analysis were conducted on a TEM microscope (JEOL 2011) at an operating voltage of 200 kV. X-ray diffraction (XRD) patterns were obtained on an X-ray diffractometer (PANalytical) at room temperature using Cu K α radiation ($\lambda = 0.15418$ nm). The accelerating voltage and the applied current were 40 kV and 80 mA, respectively. Raman spectroscopy was performed using the Renishaw spectrometer with a laser wavelength of 514 nm. Laser average power on the surface of the sample is 100 mW. The photoluminescence (PL) spectra of the samples were measured using a Spex-Fluorolog-Tau-3 spectrofluorimeter with excitation wavelength fixed at 330 nm.

2.4 UV photodetector characterization

The typical *I*–*V* characteristics and transient response of the UV photodetector fabricated from the ZnO-MWCNT hybrid paper were measured using a HP4155B semiconductor parameter analyser and a UV LED with centre peak wavelength at 335 nm. The output optical power of the 335 nm UV LED was adjusted by a current injection controller and verified using a commercial Si photodetector. The photoresponsivity of the devices were measured by Shimadzu UV-Vis 2550 spectrophotometer in connection with a Newport 1928-C optical power meter.

2.5 Photocatalytic performance testing

The thorn-like ZnO-MWCNT hybrid paper (2 cm × 2 cm) was immersed into 50 mL RhB solution with a concentration of 5 mg L⁻¹. A 150 W xenon lamp was employed as the UV light source. The distance between the sample and lamp was 10 cm. In order to be able to compare the photocatalysts, the irradiation areas for all the samples were kept the same. The changes of UV-visible spectra for the photodegradation process were measured using Shimadzu UV-Vis 2550 spectrophotometer with a deuterium lamp (190–390 nm) and a halogen lamp (280–1100 nm).

3. Results and discussion

3.1 Material characterization

A schematic illustration showing the fabrication process of the flexible thorn-like ZnO-MWCNT hybrid paper is presented in Fig. 1a. First, the fabrication process started from a bare MWCNT paper and its scanning electron microscope (SEM)

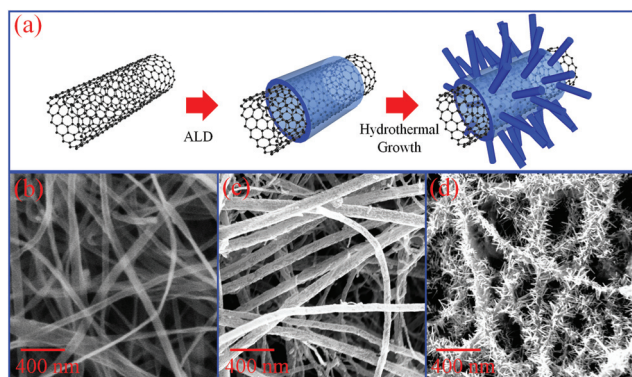


Fig. 1 (a) Schematic illustration showing the fabrication process of the flexible thorn-like ZnO-MWCNT hybrid paper. High resolution scanning electron microscopy (SEM) images of the sample in each fabrication step: (b) bare MWCNT paper, (c) MWCNT paper covered by a thin and uniform ZnO seed layer using ALD, and (d) thorn-like ZnO-MWCNT hybrid paper formed after hydrothermal growth.

image is shown in Fig. 1b. Then, a thin layer of ZnO shell was grown directly on MWCNT paper using ALD process. It is clear from Fig. 1c that the ZnO shell is uniformly coated onto the MWCNT paper that has a very high aspect ratio. The thin ZnO shell serves as a seed layer for the following hydrothermal growth step. Fig. 1d shows the SEM image of the thorn-like ZnO-MWCNT hybrid structure formed after the hydrothermal growth. Clearly, the thorn-like ZnO-MWCNT hybrid paper has very high surface to volume ratio, which is favorable for photodetector and photocatalyst applications.

The SEM image of the flexible thorn-like ZnO-MWCNT hybrid paper is shown in Fig. 2a and inset is the digital photo of the hybrid paper. The SEM and transmission electron microscope (TEM) images of single ZnO-MWCNT hybrid structure are shown in Fig. 2b and 2c, respectively, illustrating the

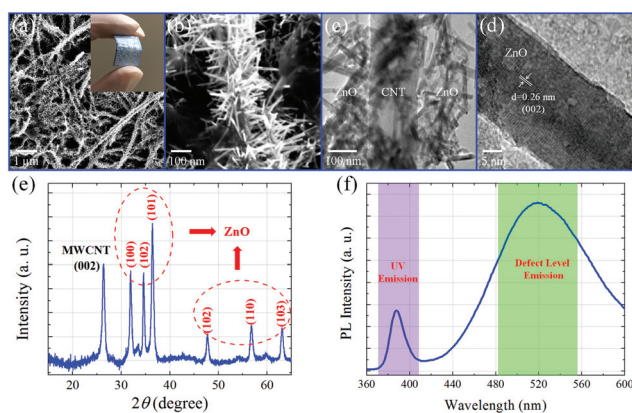


Fig. 2 (a) SEM image showing the surface of the thorn-like ZnO-MWCNT hybrid paper. Inset: Digital photo of the flexible thorn-like ZnO-MWCNT hybrid paper. (b) SEM image of a single thorn-like ZnO-MWCNT hybrid structure. (c) TEM images of a single ZnO-MWCNT hybrid structure. (d) HRTEM image of a single ZnO branch grown on the MWCNT paper. (e) XRD pattern and (f) PL spectrum of the flexible thorn-like ZnO-MWCNT hybrid paper.

excellent coverage of ZnO branches over a single MWCNT and the high aspect ratio of the ZnO-MWCNT hybrid structure. The high resolution TEM (HRTEM) image of a single ZnO branch grown on the MWCNT paper is shown in Fig. 2d, from which the lattice spacing of the ZnO branches is determined to be ~ 2.6 Å, corresponding to the distance between the (0002) planes in the wurtzite ZnO crystal lattice. The X-ray diffraction (XRD) pattern of the thorn-like ZnO-MWCNT hybrid paper is shown in Fig. 2e. All the peaks are identified and assigned according to the Joint Committee of Powder Diffraction Standards (JCPDS) data. The MWCNT has a sharp (002) peak centered at 2 theta around 26.2 degree. The remaining peaks can be well indexed to the wurtzite ZnO (JCPDS #36-1451). The room temperature photoluminescence (PL) spectrum of the thorn-like ZnO-MWCNT hybrid paper is shown in Fig. 2f. When excited at 330 nm, the PL spectrum of the thorn-like ZnO-MWCNT hybrid paper shows two bands. The band centered at 386 nm is the band edge emission of ZnO while the second band centered at 520 nm is the defect level emission due to the surface oxygen vacancy defects of the ZnO.³ These oxygen vacancy defects often dominate the electronic/chemical properties and the oxygen molecule adsorption/desorption behaviors of metal oxides.²⁴

3.2 UV photodetector characterization

To investigate the optoelectronic properties of the thorn-like ZnO-CNT hybrid paper, an UV photodetector was fabricated by deposition of interdigitated aluminium (Al) contacts with thickness of 400 nm on the surface of the hybrid paper using an electron beam evaporator. The schematic illustration of the photodetector is shown in Fig. 3a.

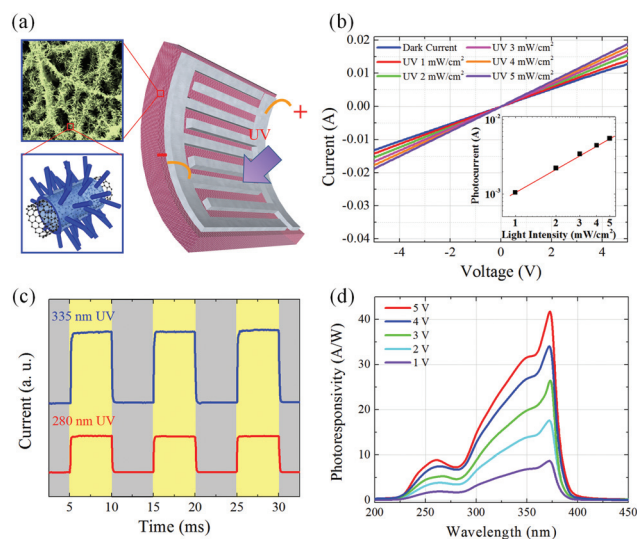


Fig. 3 (a) Schematic illustration of the UV photodetector fabricated from the ZnO-MWCNT hybrid paper. (b) Typical I - V characteristics of the UV photodetector measured with varying light intensity. The inset shows the power-dependent photocurrent of the device at -5 V bias under UV illumination. (c) Transient response and (d) photoresponsivity spectra of the UV photodetector.

The typical I - V characteristics of the UV photodetector were measured under dark and with UV illumination at 335 nm with varying light intensities, as shown in Fig. 3b. The dark current is linear, demonstrating that good Ohmic contacts are formed on the thorn-like ZnO-MWCNT hybrid paper. Upon UV illumination, the photogenerated current can be well observed. As shown in the inset of Fig. 3b, the relationship between the photocurrent and the light intensity is linear. The transient response of the UV photodetector was measured by turning on and off UV LEDs with center peak wavelengths at 335 and 280 nm, as shown in Fig. 3c. The rise time and fall time of the photodetector were measured to be around 29 and 33 ms, respectively. This is at least two orders of magnitude faster than ZnO nanomaterials based UV photoconductors.⁴ The fast transient response originates from the efficient carrier separation at the ZnO-MWCNT interface and the high carrier mobility of the MWCNT. The electron affinity for ZnO is 4.2 eV and the work function of the MWCNT is known to be 4.3–5.1 eV below the vacuum level.^{25,26} Thus, when ZnO contacting with MWCNT, it is energetically favorable for the photogenerated electron to transfer from the conduction band of ZnO to the MWCNT. Since MWCNT has much higher carrier mobility than ZnO, less accumulation of the electrons on the MWCNT side is expected. Therefore, the carrier transport efficiency can be greatly improved, leading to a fast rise of the photocurrent. When UV illumination is turned off, the excess electrons in the MWCNT can transfer to the ZnO side for recombination with holes, which is inherently a fast process.²⁷ Thus fast decay was observed for ZnO-MWCNT hybrid paper.

The photoresponsivity spectra of the thorn-like ZnO-MWCNT hybrid paper, defined as the photocurrent per unit incident optical power, are shown in Fig. 3d. Note that the photoresponsivity spectra have three peaks, which may due to the quantum confinement effect in the ZnO branches.²⁸ A maximum photoresponsivity 39.55 A W^{-1} at 375 nm was observed under 5 V bias, which is more than three orders of magnitude larger than those of commercial GaN or SiC photodetectors ($<0.2 \text{ A W}^{-1}$),⁴ demonstrating its outstanding UV sensing properties. The external quantum efficiency (EQE) of the photodetector was calculated using the equation: $\text{EQE} = R \times h\nu/q$, where $h\nu$ is the energy of the incident photon in electron volts, q is the electron charge and R is the photoresponsivity of the UV photodetector. A maximum EQE of 14927% has been achieved for 375 nm UV light. The high EQE of the hybrid paper originates from recirculation of electrons during the lifetime of the holes that are trapped and recombined with negative charged oxygen ions on the surface of ZnO. The schematic illustration showing the carrier generation and transport process in the ZnO-MWCNT hybrid paper has been presented in Fig. 4.

It has been well known that oxygen molecules adsorbs on the oxide surface and capture the free electrons present in the n-type metal oxide semiconductors, $[\text{O}_2(\text{g}) + \text{e}^- \rightarrow \text{O}_2^-(\text{ad})]$, forming a low-conductivity depletion layer near the surface of ZnO, as shown in Fig. 4a. For the thorn-like ZnO-MWCNT hybrid paper, there is a high density of hole-trap states on the

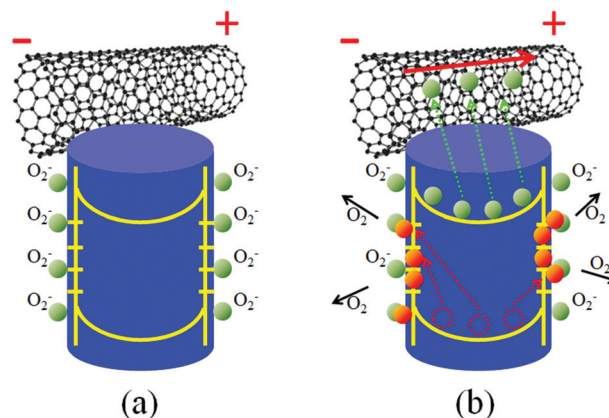


Fig. 4 Trapping and photoconduction mechanism in the ZnO-MWCNT hybrid paper: (a) When in the dark, oxygen molecules are adsorbed onto the surface of ZnO branches and capture free electrons, forming a low-conductivity depletion layer near the surface of ZnO branches. The energy band of a ZnO branch indicates band-bending and surface trap states. (b) Under UV illumination, photogenerated holes migrate to the surface and are trapped, leaving behind unpaired electrons in the ZnO that transfer to the MWCNT and are finally collected contributing to the photocurrent.

surface due to its high surface-to-volume ratio.²⁹ Under irradiation with photon energy larger than the bandgap of ZnO, electron-hole pairs are generated and soon separated, with the holes trapped at the surface along the potential slope near the surface due to the band bending (Fig. 4b),²⁹ leaving behind unpaired electrons that quickly transfer to the MWCNT and drift to the electrode by means of external bias voltage. The trapped holes will recombine with the negative charged oxygen ions and the neutral oxygen molecules are then desorbed from the surface of ZnO branches $[\text{O}_2^-(\text{ad}) + \text{h}^+ \rightarrow \text{O}_2(\text{g})]$, as shown in Fig. 4b. The transit time of the electrons in the MWCNT is very short because of MWCNT's high carrier mobility; while the surface oxygen molecule adsorption-desorption process usually takes a much longer time.²⁷ This leads to electron replenishment from negative biased electrode as soon as an electron reaches to the positive biased electrode. Accordingly, multiple electrons circulate in the MWCNT following a single electron-hole photogeneration, leading to a high photoconductive gain and hence high EQE.

For operation as a flexible optoelectronic device, it is important that the electrical properties of the UV photodetector under bending should be stable. The folding endurance of the UV photodetector was tested by measuring the I - V curves of the device without bending and after bending for different cycles, as presented in Fig. 5a. From the curves, it can be seen that, compared with the conductance of the flexible hybrid device without bending, the conductance endurance of the device remains almost constant after 50, 100, 150, 200, and 250 cycles of bending. We also checked the current flow through the device at six different curvatures, which can be seen from the corresponding photographs shown in the inset of Fig. 5b. The corresponding I - t curve of the flexible hybrid device under different bending states is shown in Fig. 5b.

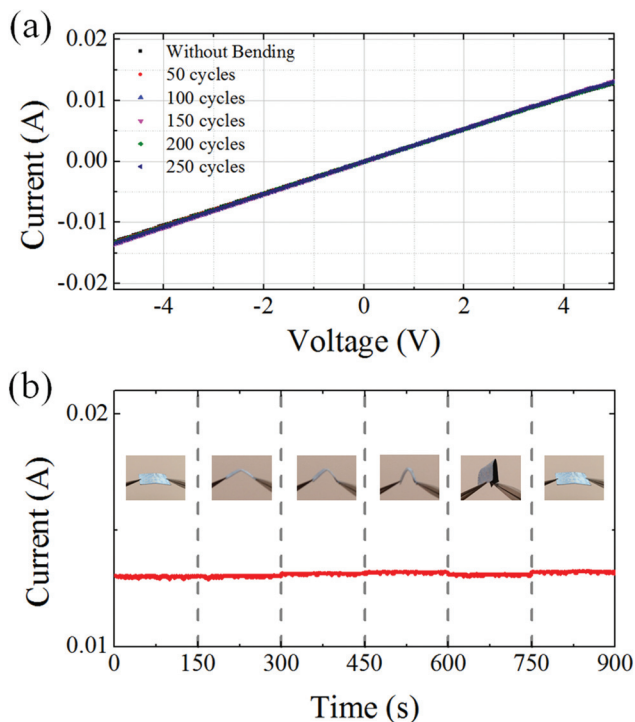


Fig. 5 (a) I - V curves of the flexible hybrid photodetector under UV illumination without bending and after 50, 100, 150, 200, and 250 cycles of bending. (b) The I - t curve of the flexible hybrid photodetector when bent with different curvatures under a bias voltage of -5.0 V. The insets are corresponding photographs of the device under the different bending states.

Clearly, the current was stable in the different bending states, revealing that the conductance of the thorn-like ZnO-MWCNT hybrid paper is minimally affected by external bending stress. These results indicate the high flexibility, folding strength, and electrical stability of the photodetector.

3.3 Photocatalytic performance testing

Inspired by the excellent UV sensing properties of the thorn-like ZnO-MWCNT hybrid paper, we also examined its application as an efficient photocatalyst. Nanostructured semiconductor photocatalysts have been widely investigated because of their promising applications in photo-degradation of polluted water.^{30–32} To utilize such photocatalysts, additional separation steps are usually necessary to remove the photocatalysts after the photo-degradation process. However, for current widely studied powder-like photocatalysts, the separation and recycling processes are challenging because of their small size-distributions. Therefore, it is necessary to develop efficient photocatalysts that possess a high surface-exposure area but also an interconnected network structure enabling easy separation after the photo-degradation process is completed. Herein, the photocatalytic properties of the thorn-like ZnO-MWCNT hybrid paper as an efficient photocatalyst was demonstrated for the degradation of RhB under UV light irradiation. Importantly, the interconnected ZnO-MWCNT network can be easily recycled from the dye solution and can be used repeatedly without performance degradation.

The photocatalytic performances of the ZnO-MWCNT hybrid paper were evaluated by photo-degradation of RhB in

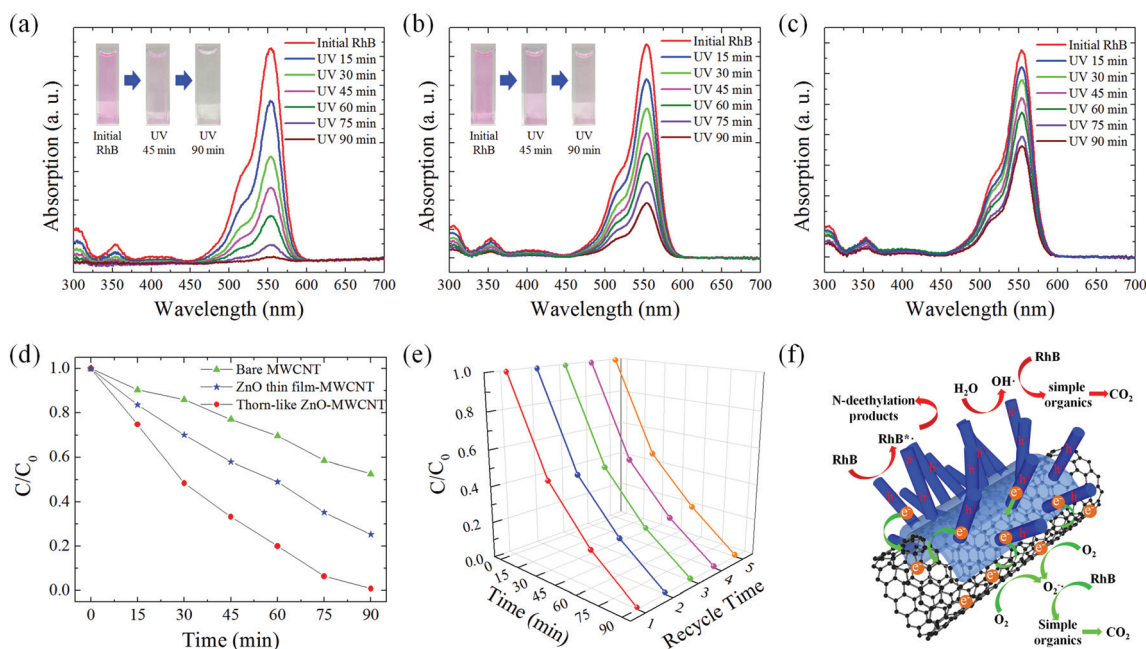


Fig. 6 UV-Vis absorption spectra changes of RhB solution in presence of (a) the thorn-like ZnO-MWCNT hybrid paper, (b) the smooth ZnO-MWCNT hybrid paper, and (c) the bare MWCNT paper under UV irradiation. Insets are digital photographs of the RhB solution after irradiation for different times. (d) Photocatalytic degradation of RhB in the presence of the three samples. (e) Recyclable photocatalytic performance of the thorn-like ZnO-MWCNT hybrid paper for the 1st, 2nd, 3rd, 4th and 5th cycles. (f) Schematic illustration of the photocatalytic mechanism of the thorn-like ZnO-MWCNT hybrid paper.

aqueous solution (RhB is a typical organic azo-dye pollutant in the textile industry). Fig. 6a shows the changes of UV-visible spectra and the colour of the RhB solutions during the degradation processes over the thorn-like ZnO-MWCNT hybrid paper. After 90 min, the RhB solution was colorless (inset in Fig. 6a) and the absorption peaks of the RhB solution in both the visible and UV region almost disappeared, indicating the excellent photocatalytic activity of the thorn-like ZnO-MWCNT hybrid paper. For comparison, the photocatalytic activities of a smooth ZnO-MWCNT hybrid paper (fabricated *via* ALD only, presented in Fig. 1c) and a bare MWCNT paper were also investigated for the RhB solution degradation under UV light irradiation and the results are shown in Fig. 6b and 6c, respectively. The corresponding plots for the concentration changes of the RhB solution determined from its characteristic absorption peak at 554 nm are shown in Fig. 6d. It is evident that the thorn-like ZnO-MWCNT hybrid paper exhibits markedly superior photocatalytic activity compared to the bare MWCNT paper and the smooth ZnO-MWCNT hybrid paper.

The recyclable photocatalytic degradation of RhB in the presence of the thorn-like ZnO-MWCNT for the 1st, 2nd, 3rd, 4th, and 5th cycles is illustrated in Fig. 6e. It should be noted that the degradation time of RhB for the 5th cycle is virtually unchanged, indicating the potential of using the thorn-like ZnO-MWCNT paper as a recyclable catalyst for the degradation of RhB under UV light irradiation. The excellent photocatalytic properties of the thorn-like ZnO-MWCNT hybrid paper can be ascribed to the efficient charge separation and the ultrahigh surface to volume ratio of the ZnO-MWCNT hybrid paper. The schematic illustration of the photocatalytic mechanism of the ZnO-MWCNT hybrid paper is presented in Fig. 6f. Under UV irradiation, photogenerated electrons will transfer quickly from the surface of ZnO to the MWCNTs, leaving a corresponding quantity of holes on the ZnO surface. Such an efficient charge separation provides direct and fast electron/hole transfer to their acceptors (H₂O, O₂, and RhB), leading to a high photodegradation efficiency.

4. Conclusions

In summary, we report fabrication of a flexible, thorn-like ZnO-MWCNT hybrid paper with high aspect ratio for efficient UV sensing and photocatalyst applications. The thorn-like ZnO-MWCNT hybrid paper was synthesized *via* atomic layer ALD of a uniform ZnO thin film on the outside surface of the MWCNT followed by hydrothermal growth of ZnO branches. The hybrid paper achieved very high surface to volume ratio, which is favorable for photodetector and photocatalyst applications. A photodetector fabricated from the hybrid paper demonstrated a high sensitivity to UV light with a maximum photoresponsivity of 45.1 A W⁻¹ at 375 nm, corresponding to an external quantum efficiency as high as 14927%. The rise time and fall time of the UV photodetector were found to be around 29 ms and 33 ms, respectively, indicating the fast transient response characteristics of the device. The high photo-

responsivity and fast transient response are attributed to the high aspect ratio, together with efficient carrier transport and collection efficiency of the hybrid paper. Besides, the thorn-like ZnO-MWCNT hybrid demonstrated excellent photocatalytic performance under UV irradiation, enabling photodegradation of organic dyes such as RhB within 90 min, with good recyclability. The fabrication method presented in this work can also be used to synthesize many other flexible functional hybrid papers based on material systems such as WO₃-MWCNT, TiO₂-MWCNT, *etc.* These functional hybrid papers may have a wide range of applications including photodetectors, optical switching, gas sensing, recyclable photocatalysts and energy storage.

Acknowledgements

The authors gratefully acknowledge support from the National Science Foundation Smart Lighting Engineering Research Center (EEC-0812056) and a NSF career award (DMR-1151028).

Notes and references

- 1 C.-Y. Chang, F.-C. Tsao, C.-J. Pan, G.-C. Chi, H.-T. Wang, J.-J. Chen, F. Ren, D. P. Norton, S. J. Pearton, K.-H. Chen and L.-C. Chen, *Appl. Phys. Lett.*, 2006, **88**, 173503.
- 2 D. C. Look, C. Coskun, B. Clafin and G. C. Farlow, *Phys. Rev. B: Condens. Matter Mater. Phys.*, 2003, **32**, 340–342.
- 3 D. Shao, M. Yu, H. Sun, T. Hu and S. Sawyer, *Nanoscale*, 2013, **5**, 3664–3667.
- 4 Y. Jin, J. Wang, B. Sun, J. C. Blakesley and N. C. Greenham, *Nano Lett.*, 2008, **8**, 1649–1653.
- 5 B. Liu, Z. Wang, Y. Dong, Y. Zhu, Y. Gong, S. Ran, Z. Liu, J. Xu, Z. Xie, D. Chen and G. J. Shen, *Mater. Chem.*, 2012, **22**, 9379–9384.
- 6 S. Wang, Y. Yu, Y. Zuo, C. Li, J. Yang and C. Lu, *Nanoscale*, 2012, **4**, 5895–5901.
- 7 J. N. Coleman, U. Khan, W. J. Blau and Y. K. Gun'ko, *Carbon*, 2006, **44**, 1624–1652.
- 8 S. Park, M. Vosguerichian and Z. Bao, *Nanoscale*, 2013, **5**, 1727–1752.
- 9 H. Lu and W. M. Huang, *Appl. Phys. Lett.*, 2013, **102**, 231910.
- 10 Y. Cheng, S. Lu, H. Zhang, C. V. Varanasi and J. Liu, *Nano Lett.*, 2012, **12**, 4206–4211.
- 11 C. S. Chen, T. G. Liu, L. W. Lin, X. D. Xie, X. H. Chen, Q. C. Liu, B. Liang, W. W. Yu and C. Y. Qiu, *J. Nanopart. Res.*, 2013, **15**, 1295.
- 12 C. Li, C. Li, Y. Di, W. Lei, J. Chen and Y. Cui, *ACS Appl. Mater. Interfaces*, 2013, **5**, 9194–9198.
- 13 P.-H. Wang, B. Liu, Y. Shen, Y. Zheng, M. A. McCarthy, P. Holloway and A. G. Rinzler, *Appl. Phys. Lett.*, 2012, **100**, 173514.

- 14 Y. Zhu, H. I. Elim, Y.-L. Foo, T. Yu, Y. Liu, W. Ji, J.-Y. Lee, Z. Shen, A. T.-S. Wee, J. T.-L. Thong and C.-H. Sow, *Adv. Mater.*, 2006, **18**, 587–592.
- 15 D. Shao, M. Yu, J. Lian and S. Sawyer, *Appl. Phys. Lett.*, 2012, **101**, 211103.
- 16 R. Zhang, L. Fan, Y. Fang and S. Yang, *J. Mater. Chem.*, 2008, **18**, 4964–4970.
- 17 T. Ikuno, T. Yasuda, S. Honda, K. Oura and M. Katayama, *J. Appl. Phys.*, 2005, **98**, 114305.
- 18 H. Kim and W. Sigmund, *Appl. Phys. Lett.*, 2002, **81**, 2085–2087.
- 19 N. Zhang, J. Sun, D. Jiang, T. Feng and Q. Li, *Carbon*, 2009, **47**, 1214–1219.
- 20 J. W. Liu, X. J. Li and L. M. Dai, *Adv. Mater.*, 2005, **18**, 1740–1744.
- 21 S. M. George, *Chem. Rev.*, 2010, **110**, 111–131.
- 22 D. Shao, X. Sun, M. Xie, H. Sun, F. Lu, S. M. George, J. Lian and S. Sawyer, *Mater. Lett.*, 2013, **112**, 165–168.
- 23 R. G. Gordon, D. Hausmann, E. Kim and J. Shepard, *Chem. Vap. Deposition*, 2003, **9**, 73–78.
- 24 R. Schaub, E. Wahlstrom, A. Ronnaus, E. Laegsgaard, I. Stensgaard and F. Besenbacher, *Science*, 2003, **299**, 377–379.
- 25 L. J. Brillson and Y. Lu, *J. Appl. Phys.*, 2011, **109**, 121301.
- 26 H. Ago, T. Kugler, F. Cacialli, W. R. Salaneck, M. S. P. Shaffer, A. H. Windle and R. H. Friend, *J. Phys. Chem.*, 1999, **B103**, 8116–8121.
- 27 D. Shao, M. Yu, J. Lian and S. Sawyer, *Appl. Phys. Lett.*, 2013, **102**, 021107.
- 28 Y. Gu, I. L. Kuskovsky, M. Yin, S. O'Brien and G. F. Neumark, *Appl. Phys. Lett.*, 2004, **85**, 3833–3835.
- 29 C. Soci, A. Zhang, B. Xiang, S. A. Dayeh, D. P. R. Aplin, J. Park, X. Y. Bao, Y. H. Lo and D. Wang, *Nano Lett.*, 2007, **7**, 1003–1007.
- 30 D. Chen and J. H. Ye, *Adv. Funct. Mater.*, 2008, **18**, 1922–1928.
- 31 Z. Zhou, Y. Lin, P. Zhang, E. Ashalley, M. Shafa, H. Li, J. Wu and Z. Wang, *Mater. Lett.*, 2014, **131**, 122–124.
- 32 J. Xu, Y. G. Zhu, H. T. Huang, Z. Xie, D. Chen and G. Z. Shen, *CrystEngComm*, 2011, **13**, 2629–2635.